doi:10.1111/evo.14171

Pushing the boundary? Testing the "functional elongation hypothesis" of the giraffe's neck

Marilena A. Müller,[1] Luisa J. F. Merten,[1] Christine Böhmer,[2,3,*] and John A. Nyakatura[1,4,*]

[1]*AG Vergleichende Zoologie, Institut für Biologie, Humboldt-Universität zu Berlin, Berlin 10115, Germany*

[2]*UMR 7179 CNRS/MNHN, Département Adaptations du Vivant, Muséum National d'Histoire Naturelle, Paris 75005, France*

[3]*Department für Geo- und Umweltwissenschaften und GeoBio-Center, Ludwig-Maximilians-Universität München, München 80333, Germany*

[4]*E-mail: john.nyakatura@hu-berlin.de*

Received April 23, 2020
Accepted January 8, 2021

Although giraffes maintain the usual mammalian cervical number of seven vertebrae, their first thoracic vertebra (T1) exhibits aberrant anatomy and has been hypothesized to functionally elongate the neck. We test this "functional elongation hypothesis" by combining phylogenetically informed analyses of neck length, three-dimensional (3D) vertebral shape, and of the functional significance of shape differences across a broad sample of ruminants and camelids. Digital bone models of the cervicothoracic transition were subjected to 3D geometric morphometric analysis revealing how the shape of the seventh cervical (C7) has converged in several long-necked species. However, we find a unique "cervicalization" of the giraffe's T1. In contrast, we demonstrate a "thoracalization" of C7 for the European bison. Other giraffids (okapi and extinct *Sivatherium*) did not exhibit "cervicalized" T1 morphology. Quantitative range of motion (ROM) analysis at the cervicothoracic transition in ruminants and camelids confirms the "functional elongation hypothesis" for the giraffe in terms of increased mobility, especially with regard to dorsoventral flexion/extension. Additionally, other factors related to the unique morphology of the giraffe's cervicothoracic transition such as neck posture and intervertebral stability are discussed and should be considered in future studies of giraffe neck evolution.

KEY WORDS: Camelidae, Cetartiodactyla, geometric morphometrics, range of motion, Ruminantia, vertebral column.

The neck of the giraffe (*Giraffa camelopardalis*: Mammalia, Ruminantia) is an icon of evolutionary biology. Its exceptional length is achieved while adhering to the mammalian "rule of seven" cervical vertebrae (Flower and Gadow 1885; Simmons and Scheepers 1996; Mitchell and Skinner 2003; Van Sittert et al. 2010; Arnold et al. 2017). Goethe (2012) and Owen (1866) already were familiar with the puzzling observation and maintenance of just seven but extraordinary elongate cervicals in the giraffe. Lankester (1908) was the first to note structural differences of the cervicothoracic transition in giraffes in comparison to other mammals and proposed a functional elongation of the neck. This "functional elongation hypothesis" posits that while maintaining a count of seven cervicals, the first thoracic vertebra (T1) has been functionally incorporated into the giraffe neck despite maintaining its thoracic (i.e., rib-bearing) identity.

Specifically, Lankester (1908) qualitatively compared the cervical shape of giraffes to other mammal species. The author found that in the okapi and other ungulates, the articulation between the seventh cervical (C7) and T1 changes (from laterally facing zygapophyseal facets to medially facing zygapophyseal facets), whereas in the giraffe this change in the articulation pattern occurs between T1 and T2. Lankester's "functional elongation hypothesis" has been substantiated by recent evidence for unique musculoskeletal features in agreement with increased mobility at the giraffe's cervicothoracic transition (Gunji and Endo 2016). Solounias (1999) reinvestigated Lankester's observations

[*]CB and JAN contributed equally to this work.

and noted that many anatomical characters of the giraffe are located one vertebra posteriorly compared to other mammals (e.g., roots of the brachial plexus and insertion of thoracic longus colli muscles). He proposed that the giraffe escapes from the "rule of seven" and possesses eight cervical vertebrae with insertion of an additional vertebra between C2 and C6 (Solounias 1999). In contrast to a homeotic variation (i.e., the transformation of one morphology into another), a change in the number of segments is referred to as a meristic variation (Bateson, 1894). Mitchell and Skinner (2003) and Badlangana and Adams (2009) criticized this idea based on the articulation of a rib on the giraffe's T1 that attaches directly to the sternum—the defining characteristic of a thoracic vertebra. However, all authors agree that T1 of the giraffe appears to be a transitional vertebra, because of its short spinous process compared to other thoracic vertebrae. Moreover, T1 is considered "semicervical" because its postnatal growth exponent is between that of the cervical series (faster growth) and the thoracic series (slower growth) (van Sittert et al. 2010). Unexpectedly, Danowitz et al. (2015b) found that elongation of the neck preceded the origin of the Giraffidae perhaps hinting at neck elongation occurring within the Pecora, a clade of ruminants nested within the Cetartiodactyla. In light of this debate, it is necessary to revisit shape evolution of the neck-trunk transitional region of giraffes using methodology that accounts for three-dimensional (3D) vertebral shape, morphofunctional consequences, and for phylogenetic context. These new data will allow us to elucidate this long-standing evolutionary conundrum.

To test the "functional elongation hypothesis" of giraffe neck evolution, the shapes of the vertebrae making up the cervicothoracic transition (C7 and T1) of 37 species representing all major lineages of Ruminantia, and, for comparison due to their relatively long necks, the Camelidae (Mammalia, Cetartiodactyla) were analyzed (Fig. 1). We tested for a relationship of shape changes with relative neck length and also conducted "virtual experiments" using digital 3D surface models of the vertebrae to assess the range of motion (ROM) between C7 and T1 to characterize specifics of neck elongation in giraffes in contrast to other relatively long-necked species as well as to all other species analyzed. A phylomorphospace and a phenogram were created to visualize how shape diversity of C7 and T1 as well as morphological disparity between C7 and T1 (quantified as Procrustes difference) relate to phylogeny, respectively. We then directly studied the association between the morphological data (shape, relative neck length) and the functional data (ROM) using phylogenetic generalized least squares regression (PGLS). We expected to find similarity of C7 shape shared by relatively long-necked species (see below) and quantified this potential convergence. For the giraffe, we further expected to find a diverging shape of T1 in comparison to all other species that results in increased mobility at the cervicothoracic boundary. This combination of diverging T1 shape and increased C7/T1 mobility would provide quantitative evidence for the "functional elongation hypothesis." Three-dimensional models of partially damaged *Sivatherium giganteum* cervical specimens were included in a separate analysis of vertebral shape to elucidate the form-function relationship of the cervicothoracic transition within giraffids. *Sivatherium giganteum* is a large, fossil giraffid with robust physique, but a relatively short neck (Basu et al. 2016). In contrast to the extant giraffe and due to their nonelongated necks, we hypothesized the other giraffids in our sample (okapi and *S. giganteum*) to not exhibit a combination of homeotic changes (i.e., "cervicalization" of T1) and increased C7/T1 mobility as expected for the giraffe.

Materials and Methods

SPECIMENS

Vertebrae stemming from the collections of major German natural history museums, the Koninklijke Maatschappij voor Dierkunde of Antwerp, and the Natural History Museum of London were included in this study. All analyzed specimens appeared to be skeletally mature (indicated by epiphyseal fusion). One *Camelus bactrianus* (SMF 25542) specimen lacked complete epiphyseal fusion in the vertebrae, but long bones of this specimen clearly indicated an adult individual and it was included in the analysis. No vertebrae showed any obvious pathologies. Both sexes were sampled indifferently; wild-caught animals were preferred but zoo animals were also included in the study to compose a larger dataset.

The sample includes vertebrae from 37 extant ruminant and camelid species and one extinct giraffid. A total of 108 specimens (i.e., 54 C7/T1 pairs) were included (SI 1 and 2). The vertebrae of *S. giganteum* belong to two different individuals and both were not completely preserved, but were examined using an adjusted set of landmarks (see below). In both specimens of *S. giganteum*, a part of the dorsal spinous process is missing. In the C7 specimen, the transverse process and parts of the interior costal facet are missing as well. In the T1 specimen, parts of the vertebral body and the interior costal facet are damaged (SI 3).

DATA ACQUISITION

Three-dimensional surface models of specimens were acquired using either microcomputed tomography (μCT) or photogrammetry (PH). All surface models are available on the public database MorphoMuseum (https://doi.org/10.18563/journal.m3.129; Müller et al. 2021). For μCT (YXLON FF35 CT scanner, Museum für Naturkunde, Berlin), resolution ranged from 56 to 196 μm depending on the size of the vertebrae. The raw data obtained by the CT scanner were further edited with Fiji

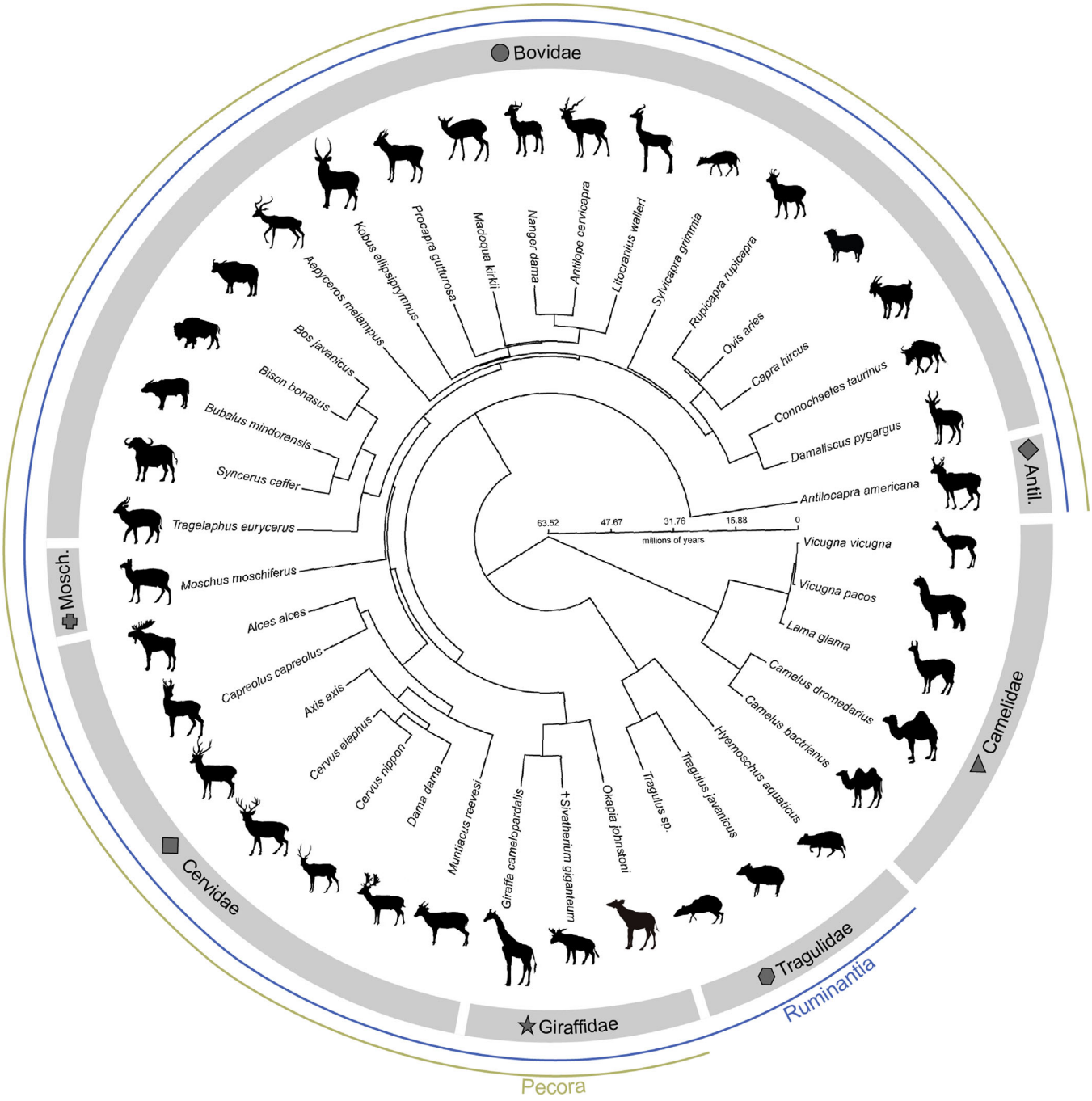

Figure 1. **Phylogeny of cetartiodactyls considered in this study. Symbols were assigned to the seven families examined (marked by gray boxes). The time-calibrated tree is based on the study by Toljagic et al. (2018). Timescale in million years ago (MYA). Antil. = Antilocapridae; Mosch. = Moschidae. See SI 2 for an overview of C7/T1 vertebrae pairs.**

plug-ins for ImageJ (version 1.51k; Schneider et al. 2012, Schindelin et al. 2012). Scans were cropped to reduce the amount of data and the contrast was increased before being saved as 16-bit binary tiff stacks (image sequences). The created tiff stacks were imported into Amira (Thermo Fisher Scientific, version 6.0.0), a software for visual data analysis (Stalling et al. 2005), and 3D bone surface models were created using the software's segmentation editor. The number of polygons was reduced to 1,000,000 consistent for all specimens.

For PH, high-resolution images were taken using a Canon EOS 1200D digital camera with 18–55 mm standard zoom lens. Specimens were fixed to a flat surface using modeling clay, and photos were taken from around the specimen. Afterward, the vertebra was turned upside-down and the process was repeated. The

images (about 70 images per specimen) were uploaded in Agisoft Metashape (version 1.5.2), an image-based 3D modeling software creating 3D objects from still images (Rcljić et al. 2019). Using the commands "align photos," "build dense cloud," and "build mesh," surface models were generated. The two resulting models (e.g., top and bottom aspects of the vertebra) were loaded into MeshLab (version 1.3.4 beta; Cignioni et al. 2008) and merged using the "alignment" function. Vertebrae C7 and T1 of *S. giganteum* were digitized at the Structure and Motion Laboratory of the Royal Veterinary College, London, using PH. Vertebrae of one specimen of *G. camelopardalis* (KMDA M-10861) were digitized at the Department of Veterinary Science, University of Antwerp, using a surface laser scanner. Both datasets were made available to us prior to the study.

To test whether the digitizing method has an influence on the results, two models of the same vertebra (C7 *Vicugna vicugna* SMF 94752) were created using μCT and PH and were included in a geometric morphometrics analysis with other specimens. The two models plot extremely close to one another in the morphospace (see SI 4). Hence, errors introduced into the analysis by the method of model creation were neglected in our analysis.

Comparative data for neck and overall vertebral column lengths were not available in the published literature for most of the species. We therefore determined relative neck length. Relative neck length was the ratio between occiput to cervicothoracic boundary distance and overall occiput-tailhead distance (SI 5). This measure was derived from lateral aspect photos of the species found on the internet with lengths measured using ImageJ (Schindelin et al. 2012).

COMPARATIVE SHAPE ANALYSIS

Vertebral shape was assessed using 3D geometric morphometrics. As vertebrae principally are bilaterally symmetrical structures, landmarks were only placed on one side (left side) of the vertebra to quantitatively evaluate morphological differences. A set of 31 landmarks was used (Fig. S6). All landmarks are type II or type III (Bookstein 1997; SI 7 for landmark definitions). To include C7 and T1 of *S. giganteum* in an additional analysis, this landmark set had to be adjusted. Because the spinous process is missing in both fossil vertebrae specimens and the transverse process is missing in C7, seven landmarks were excluded.

Three-dimensional surface models (*.ply) were loaded into IDAV Landmark (version 3.0) (Wiley et al. 2005) and landmarks were digitized on the surface of the 3D scans. Before placing landmarks, the dorsal lines of the vertebral bodies were aligned horizontally. Landmarking was performed by just one of us (MAM) to keep the error introduced through the unavoidably subjective placement of landmarks to a minimum.

The 3D coordinates of both vertebrae in each landmark set (i.e., the full landmark set and the reduced landmark set to allow inclusion of the fossil specimens) were superimposed by a generalized least squares Procrustes analysis (GPA) (Gower 1975; Rohlf and Slice 1990; O'Higgins 2000; Rohlf and Corti 2000) using Morphologika^2 (version 2.5). Because in some cases several specimens of one species' vertebrae were analyzed, these data were averaged for species-level analyses.

To examine shape variation, principal component analyses (PCA) based on the superimposed Procrustes coordinates were carried out (Jolliffe 2011). In GPA, the information about size of the specimens is preserved in centroid size (Zelditch et al. 2004). To test if shape variation is a function of size, a multivariate regression analysis (log-transformed centroid size against all PCs) was performed implemented in Morphologika^2. *XY*-plots of the first four PCs with 95% confidence ellipses were created.

The distance in the multivariate morphospace between two vertebrae was quantified using the Procrustes distance. This metric provides a measure of the morphological similarity (low Procrustes distance) and morphological disparity (high Procrustes distance), respectively, between C7 and T1, considering all dimensions. The Procrustes distances (of each vertebra) from the mean provides a measure of the morphological disparity within the sample. It quantifies how morphologically similar or different the vertebrae are depending on their position (C7 and T1, respectively). The "morphol.disparity" function from the R package "geomorph" (Adams et al. 2017) was used to test if the morphologies of C7 are significantly more diverse than that of T1 or not.

PHYLOGENETIC COMPARATIVE METHODS

Because closely related species share a recent common history, the data cannot be considered as independent (Harvey and Pagel 1991). Phylogenetic relationships from a molecular tree of Toljagic et al. (2018) were used. The time-calibrated tree was pruned to the 37 extant species that were sampled for our analyses. The resulting tree was used in all following phylogenetically informed analyses. Phylogenetically informed analyses were performed using the software R version 3.6.3 (respective packages are indicated below) (R Development Core Team, 2019). The fossil *S. giganteum* was considered the sister taxon to the extant giraffe (*G. camelopardalis*) based on Danowitz et al. (2015a).

The "phylomorphospace" function in the R package "phytools" (Revell 2012) was used to project the phylogenetic tree into the morphospace resulting from the PCA (Sidlauskas 2008). A phenogram using the Procrustes distance between C7 and T1 was built with the function "phenogram" from the R package "phytools" (Revell 2012) to visualize morphological disparity in relation to phylogeny. The phylogenetic signal in univariate data (i.e., neck length, ROM) was estimated using Blomberg's *K* (Blomberg et al. 2003) with the function "phylosig" in the R package "phytools" (Revell 2012). The degree of phylogenetic

signal in the multivariate data (i.e., Procrustes shape variables) was estimated using the multivariate version of Blomberg's *K*-statistic (K_{mult}: Adams 2014) with the function "physignal" in the R package "geomorph" (Adams et al. 2017). It allowed us to test whether the same trait properties are present in related taxa more frequently than expected by Brownian motion (Blomberg et al. 2003).

Distantly related, putative convergent taxa fall closer to one another in morphospace than to their relatives (Stayton 2006). To test for convergent evolution in vertebral shape, we used the R package "convevol" (Stayton 2017). Morphospace was defined as the first three PC axes of the shape analysis for this analysis (about 87% of total variance explained); subsequent PC axes each contribute less than 5% of the variance. The function "convrat" quantifies the degree of convergence providing the measure C_1 (Stayton 2015). C_1 represents the proportion of the maximum distance between the lineages that have been brought together by subsequent evolution. It ranges from 0 (i.e., not convergent at all) to 1 (i.e., fully convergent) (Stayton 2015). The significance of convergence (as quantified by 'convrat') was evaluated using the "convratsig" function (500 simulations).

RANGE OF MOTION

To assess ROM at the cervicothoracic transition (i.e., between C7 and T1) of all 37 extant species, 3D bone models were imported into Autodesk Maya (version 2016) and arranged in the osteological neutral pose (ONP; SI 8). Following Vidal et al. (2020), the ONP is defined as the full articulation of the zygapophyseal facets, with complete overlap of the facet outlines in all three anatomical planes (anteroposterior, lateral-medial, and dorsoventral). These authors further detail that zygapophyseal joint capsules are not thicker than a flat sheet with the same outline as the bony facet and argue that using the zygapophyses to define a neutral pose is better suited than using the intervertebral soft tissue at the vertebral centra (Vidal et al. 2020).

A center of rotation was found by fitting (i.e., manually adjusting size and position) a semitransparent sphere matching the curvature of the zygapophyseal facets of C7 with the sphere's surface from the lateral and dorsal perspectives (see Kuznetsov and Tereschenko, 2010; Belayaev et al. 2020 for a similar approach of using zygapophyseal curvature; SI 8). Next, a Maya "joint" is placed into the center of the fitted sphere (cf. Arnold et al. 2014), with the axes of the joint set to match the anteroposterior, lateral-medial, and dorsoventral axes of T1. Articulation of the capitulum of the first rib usually spans the cervicothoracic transition and is composed of the caudal costal facet on C7 and the cranial costal facet on T1 (both facets are thus also referred to as demi-facets). To account for potential limitations in ROM due to the presence of the rib at the cervicothoracic transition, two additional spheres were fitted (one on each body side) into the costal facets to model the capitulum of the left and right first rib.

To finally derive ROM as osteologically plausible dorsoventral flexion/extension, lateral bending, and intervertebral torsion, we virtually moved the 3D bone model of an individual's C7 relative to the individual's T1 (SI 8). ONP was used as a reference pose for ROM measurement. The angle (in degree) of deflection was measured using the Maya "joint" (cf. Arnold et al. 2014; Nyakatura et al. 2015). Movement was considered implausible when either (i) C7 post- and T1 prezygapophyses were no longer overlapping (Taylor and Wedel, 2013; Krings et al. 2017) or (ii) when bone collisions occurred in the model (Pierce et al. 2012; Arnold et al. 2014; Nyakatura et al. 2015; Manafzadeh and Padian 2018; Regnault and Pierce, 2018; Nyakatura et al. 2019; Manafzadeh and Gatesy 2020).

Bone collisions were identified by one of us (LM) and the degree of possible deflection (positive and negative rotation around each of the three anatomical axes) was quantified separately. The sum of all plausible movements was defined as cumulative ROM. This methodology does not account for soft tissues that had been demonstrated to further restrict mobility (Arnold et al. 2014; Manafzadeh and Padian 2018). However, assessment of ROM using bone models derived from museum collections allows to effectively include a larger number of specimens (no cadavers needed) and often even fossils. Unfortunately, specimens of *S. giganteum* could not be included in this analysis, because alignment of the zygapophyses was impossible as specimens likely stem from different individuals.

The significance of the observed shape changes at the cervicothoracic transition associated with neck length and ROM was evaluated by performing a phylogenetic generalized least squares regression (PGLS) on the aligned Procrustes coordinates using the function "procD.pgls" (1000 random permutations) ("geomorph" package in R; Adams et al. 2017).

Results

COMPARATIVE SHAPE ANALYSIS

In the 3D geometric morphometric analysis of the two cervicothoracic vertebrae (C7 and T1) for 37 ruminant and camelid species, the first two principal components (PCs) together explain 82% of the total variance in shape (Fig. 2A). PC1 (71%) reflects changes in the length of the vertebral body and the height of the spinous process (longer processes and shorter bodies with increasing PC score). PC2 (11%) especially shows alterations in the inclination of the spinous processes (more cranial orientation with increasing PC score). PC3 explains 5% of the variance (mainly related to changes in the length of the vertebral arch); all other PCs had eigenvalues of less than 5% (SI 9). Ninety-five percent of the total variance in shape is explained by the first 11

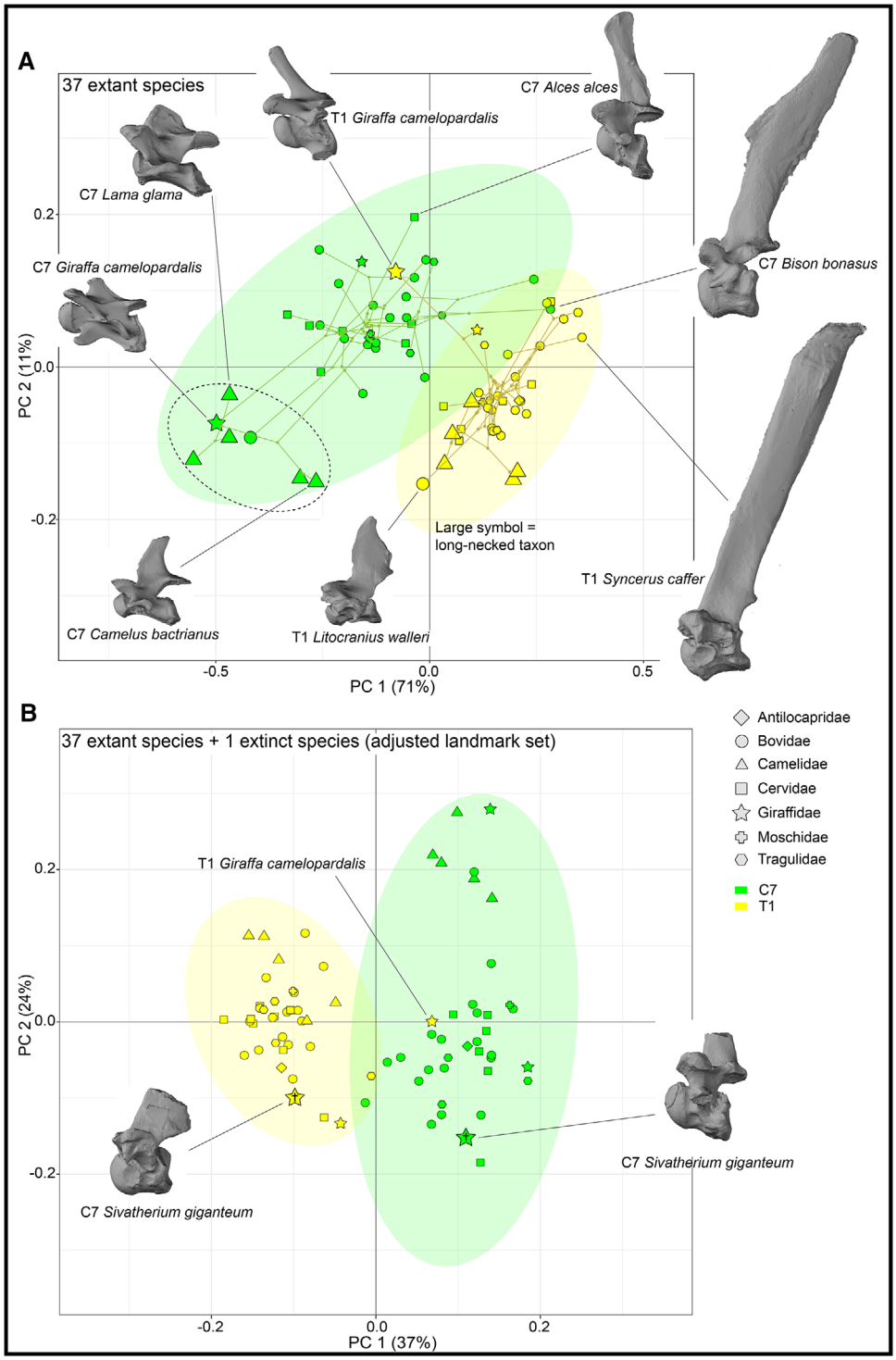

Figure 2. Three-dimensional shape analysis of vertebrae at the cervicothoracic transition (C7 and T1) in representatives of ruminants and camelids. (A) PC1/PC2 scatter plot of PCA using the full landmark set (37 extant species) with 95% confidence ellipses. The phylogeny is projected into the morphospace. The dotted ellipse highlights the convergent occupation of the morphospace by C7 vertebrae of long-necked species (Camelidae, *Giraffa camelopardalis*, and bovid *Litocranius walleri*). Lateral views of vertebrae models (scaled to approximately same size of vertebral centrum) illustrate shape changes across the morphospace. (B) PC1/PC2 scatter plot of PCA using the adjusted landmark set (37 extant species and damaged specimens of *Sivatherium. giganteum*). Note that T1 of *Giraffa camelopardalis* plots outside the 95% confidence ellipse in panels A and B.

Table 1. Phylogenetic generalized least squares (PGLS) regression results for the cervicothoracic transition.

Regression model	df	SS	*F*-value	r^2	*Z*	*P*-value
C7 shape∼ROM	1	0.221	3.127	0.084	2.005	0.022*
C7 shape∼neck length	1	0.178	2.480	0.068	1.642	0.044*
T1 shape∼ROM	1	0.215	2.495	0.068	2.495	0.083
T1 shape∼neck length	1	0.103	1.147	0.033	1.147	0.292
Procrustes distance C7-T1∼ROM	1	0.032	11.674	0.256	1.731	0.008*
Procrustes distance C7-T1∼neck length	1	0.093	96.877	0.740	2.486	0.001*
Neck length∼ROM	1	58.306	10.606	0.238	1.628	0.007*

PCs (SI 10). The phylogenetic signal considering all Procrustes shape variables was statistically significant, but low for C7 ($K_{mult} = 0.35$, $P = 0.001$) and for T1 ($K_{mult} = 0.46$, $P = 0.046$). Multivariate regression revealed that allometry accounts for about 0.98% of total variance (Wilks' lambda = 0.76, $F = 1.77$, $P = 0.079$). The 95% confidence ellipses of PC1 and PC2 of C7 and T1 slightly overlap (Fig. 2A). Due to their large vertebral bodies and short spinous processes, the cervical vertebrae plot further left and the thoracic vertebrae with relatively short vertebral bodies and long spinous processes further right (along PC1). The morphological variance in C7 is greater than in T1 (Procrustes variance: C7 = 0.084, T1 = 0.049, $P = 0.023$). The C7 of relatively long-necked species (all camelids, the gerenuk, and the giraffe have a relative neck length of ≥50%; SI 5) occupies a common area of the morphospace of PC1 (Fig. 2A). Testing the hypothesis that long-necked species convergently evolved similar C7 morphology revealed moderate but significant convergence when considering PC1-3 ($C_1 = 0.351$, $P = 0.005$). By comparison, we did not find evidence for considerable convergent evolution of T1 morphology of long-necked species ($C_1 = 0.108$, $P = 0.464$).

T1 of the giraffe plots clearly apart from the other T1 examined in this analysis and falls within the 95% confidence ellipse of the cervical vertebrae. It is the only thoracic vertebra not falling into the 95% confidence ellipse of our dataset. Noticeably, C7 of *Bison bonasus* (the European bison) plots within the 95% confidence ellipse of T1 and is the only C7 falling out of the C7 95% confidence ellipse in the PC1-PC2 scatter plot. PC3 and PC4 reveal shape alterations in the length of the vertebral arch (PC3) and the height of the vertebral body (PC4) (SI 9). Overall shape differences between C7 and T1 are reflected in Procrustes distances between these two bones of each species (Fig. 3). The largest distances between C7 and T1 were found in the Camelidae and the giraffe (also note the large phenotypical difference between okapi and giraffe that evolved in relatively little time; Fig. 3). The smallest differences between both vertebrae were found in the European bison. PGLS reveals that the shape difference between C7 and T1 is significantly explained by relative neck length ($P = 0.001$; Table 1).

COMPARATIVE SHAPE ANALYSIS INCLUDING *SIVATHERIUM*

Analysis of vertebrae of the cervicothoracic transition (C7 and T1) including *S. giganteum* was conducted using an adjusted landmark set due to missing parts in the fossil specimens. About 60% of the variance is explained by PC1 and PC2 (Fig. 2B). Here, PC1 (37%) reflects alterations in the size of the zygapophyses and the inclination of the neural arch. PC2 (24%) depicts changes in the height of the neural arch and the length of the vertebral body. PC3 explains 10% of the variance (SI 9); all other PCs had eigenvalues of less than 5%. Ninety-five percent of the total variance in shape is explained by the first 19 PCs (SI 10). Nevertheless, the 95% confidence ellipses of C7 and T1 only slightly overlap in the PC1 versus PC2 scatterplot (Fig. 2B), too. C7 and T1 of *S. giganteum* plot within the respective 95% confidence ellipses and plot closer to the okapi than to the giraffe. Even without the consideration of the spinous and transverse processes, T1 of the giraffe plots outside the 95% confidence ellipse of T1 within the morphospace of C7 and differs clearly from the thoracic vertebrae of all other species in this analysis, too.

ROM BETWEEN C7 AND T1

Cumulative ROM showed a statistically significant phylogenetic signal ($K = 0.81$, $P = 0.001$) and was largely determined by dorsoventral flexion/extension (SI 5). Sister taxa tend to share similar intervertebral mobility, whereas less closely related taxa are more (functionally) divergent (Fig. 3). The giraffe is a notable exception to this overall pattern and deviates substantially from its closest extant relative, the okapi, in terms of mobility. Additionally, larger values for cumulative ROM were often found in species with larger differences in shape between C7 and T1 (e.g., in the Camelidae and the giraffe). In contrast, smaller values tended to be found in species with high similarity in C7/T1 shape. The giraffe was found to have the second largest cumulative ROM (65.2°) and the largest dorsoventral flexion/extension mobility (55.2°) (SI 5). The giraffe's C7/T1 mobility was more than twice as large as in the okapi (cumulative ROM: 29.2°; dorsoventral flexion/extension: 19.4°, SI 11). The high similarity of the European bison's C7 with T1 of the other analyzed species

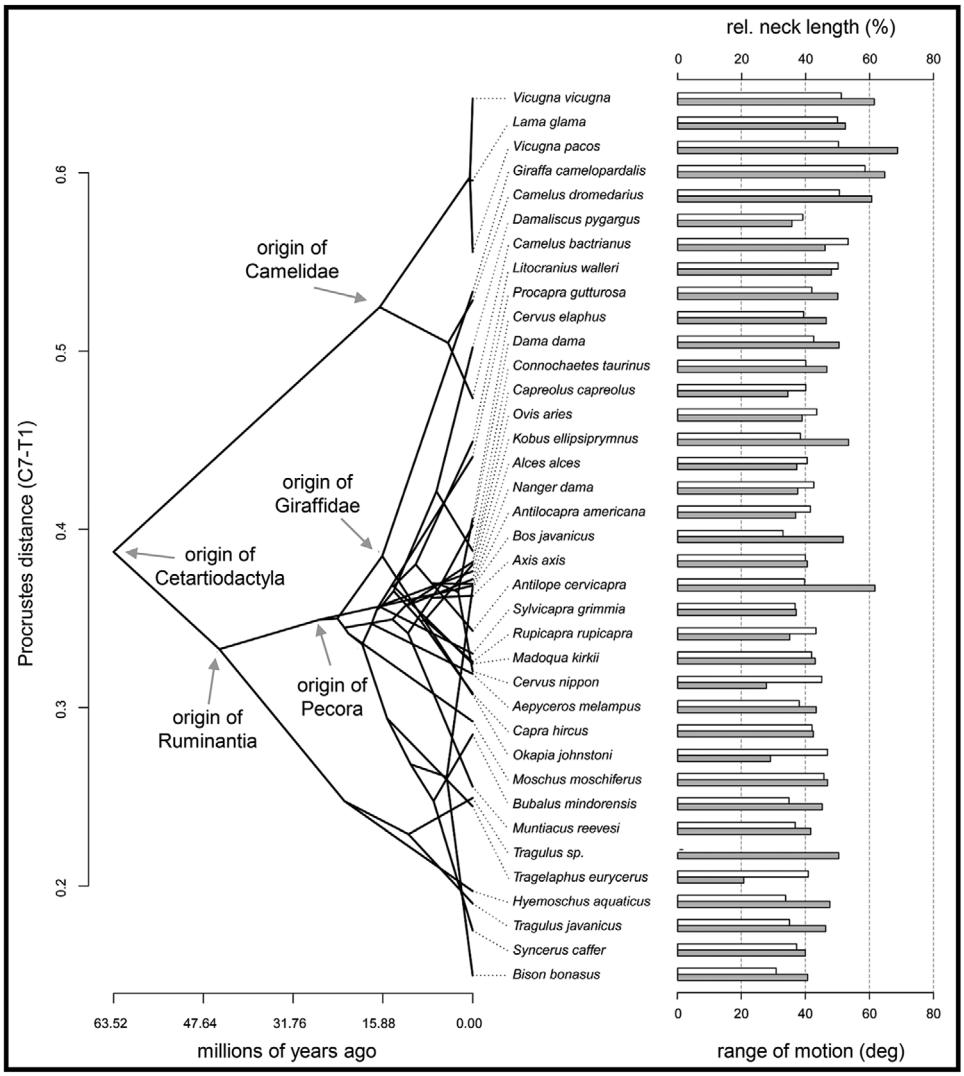

Figure 3. **Phenogram of Procrustes distances between C7 and T1 of all extant species in this study (left) and the cumulated range of motion between both vertebrae (right, gray bars) as well as relative neck length (right, white bars).**

is accompanied by a relatively low (but not the lowest) cumulative ROM. PGLS demonstrates that the shape difference between C7 and T1 is significantly explained by differences in ROM ($P = 0.008$; Table 1).

Discussion

COMBINED ANALYSIS OF 3D SHAPE AND FUNCTION CONFIRMS "FUNCTIONAL ELONGATION HYPOTHESIS"

To test the "functional elongation hypothesis," the cervicothoracic vertebral morphology of cetartiodactyl species was quantitatively examined using 3D geometric morphometrics and phylogenetically informed comparative methods. Functional significance of differences in the morphometric data was further evaluated in terms of mobility (ROM).

Using geometric morphometrics, subtle shape differences between vertebrae can be quantified (Arnold et al. 2016; Randau et al. 2017; Böhmer 2017; Jones et al. 2018; Arnold 2020). C7 and T1 of the giraffe show striking morphological differences to their respective counterparts in other cetartiodactyl species. C7 of the giraffe differs from C7 of the okapi and most other species in our dataset by a shorter spinous process and relatively larger vertebral body. Both are characteristics of more anterior cervical vertebrae (Solounias 1999; Danowitz and Solounias 2015; Gunji and Endo 2016). However, similar C7 morphology evolved in all long-necked taxa of our dataset (see below). In mammals, C7 is commonly referred to as "vertebra prominens" because of its long spinous process (Cramer and Darby 2014), but this is not present in the giraffe. Another difference to general mammal C7 morphology concerns the transverse foramen and ventral tubercles (Solounias 1999). These characteristics are present in C7 in the

giraffe, but not in C7 of other mammals. This may have functional implications considering the neck musculature. The cervical longus colli muscle (the cervical part of the major neck flexor) originates from the ventral tubercles of the cervical vertebrae. Presence of these tubercles on C7 in the giraffe thus demonstrates a homeotic shift by one vertebra (Gunji and Endo 2016). To further substantiate this notion of a homeotic shift, we additionally tested whether the C7/T1 articulation of the giraffe has a similar ROM, that is, function, as the C6/C7 articulation of the closest relative (okapi). We found that at the C6/C7 articulation, the okapi exhibits a cumulative ROM of 76.7° with similar values to the C7/T1 articulation of the giraffe for possible dorsoventral flexion/extension (53.5° in okapi vs. 55.2° in giraffe) and lateral bending (9.0° vs. 6.0°), but considerably larger values for torsion (14.2° vs. 4.0°). Ultimately, homeotic shifts as present in the giraffe (summarized in SI 12) can be assumed to be introduced through changes of the *Hox* code and have been induced experimentally in mice (Chen et al. 1998; Wellik 2009). To test this in giraffe, developmental studies in this non-model species are necessary and are thus not possible at this point (Böhmer et al. 2018).

T1 of the giraffe is most similar to C7 of the other species and shown here to differ from their respective T1 by a shorter and more anterior leaning spinous process as well as a relatively larger vertebral body and a more ball-like shape of the anterior articulating surface of the vertebral centrum (see also Lankester 1908; Badlangana and Adams 2009; Damian et al. 2013). This demonstrates that T1 of the giraffe resembles the posterior-most cervical vertebra of the other species. Additionally, we demonstrate quantitatively that C7 and T1 of the giraffe possess relatively smaller zygapophysial facets and neural arches. In studies concerned with archosaur neck anatomy, these properties were proposed to result in an increased flexibility of the cervicothoracic region, mainly allowing larger dorsoventral movements of the neck (e.g., Stevens and Parrish 2005a; Cobley et al. 2013; Krings et al. 2014; Krings et al. 2017). Finally, thoracic vertebrae of giraffe, okapi, and other ruminants and camelids usually possess three costal facets (cranial costal facet, caudal costal facet, and transverse costal facet). T1 of *G. camelopardalis*, in contrast, lacks the cranial and caudal facets and possesses an isolated facet on the lateral side of the vertebral body beneath the transverse process (Gunji and Endo 2016). This morphological feature results in (i) the first rib having contact with the isolated facet of T1 without touching the caudal part of C7 and (ii) the second rib articulating with the cranial costal facet and the transverse costal facet of T2 without contacting the caudal part of T1 (Fig. 4). Together, this condition of the giraffe's T1 provides support for the "functional elongation hypothesis" by suggesting that T1 of the giraffe adopted the kinematic function of a cervical vertebra and increased mobility to the neck (cf. Gunji and Endo 2016). These characters potentially contribute to the extreme elongation of the giraffe neck by mobilizing the anterior-most part of the thoracic vertebral column. In line with our expectation, our detailed anatomical analysis demonstrated homeotic shifts in C7 and T1 (SI 12). In addition, our functional analysis demonstrated pronounced mobility in comparison to other ruminants and camelids, especially in terms of dorsoventral flexion/extension. The giraffe exhibited the largest dorsoventral ROM of our dataset. Together, our analysis thus corroborates the "functional elongation hypothesis" of the giraffe neck-giraffes indeed are pushing the boundary.

The aberrant morphology of T1 may be related to other functions than mobility. For example, aberrant shape of the giraffe's T1 may also be related to a stabilizing function. Exceptional neck elongation is involving large moments (consider an approximately 2 m lever arm of the head's mass) at the cervicothoracic transition. Musculoskeletal adaptations as identified by Gunji and Endo (2016) could contribute to relatively large mobility while also helping to satisfy an increased demand for stabilization. The head and neck of giraffes participate in rhythmic up-and-down movements during locomotion that has been demonstrated to significantly influence the dynamics of the gait (Loscher et al. 2016; Basu et al. 2019). Additionally, the upright posture of the long neck increases the mechanical load on the skeletal elements of the cervicothoracic transition (see below). These additional potential explanations for aberrant vertebral shape should be the focus of future research, for example, by use of modeling approaches such as multibody dynamics or finite element analysis of vertebrae under load.

EVOLUTIONARY TRENDS WITHIN RUMINANTIA AND CAMELIDAE

Although Danowitz and Solounias (2015) described the C7 of the giraffe as "unique not only to giraffids but also to mammals," the present study demonstrates that concerning the main shape differences, other long-necked ruminants such as *Litocranius walleri* (the gerenuk) and camelids exhibit similar specializations in C7 as the giraffe (longer vertebral bodies, shorter and rather posterior sloping spinous processes) contrasting the other species in our sample (Fig. 4A). Our quantitative analysis found a significant albeit moderate convergence between the C7 shape of the long-necked species of Cetartiodactyla. The convergent shape thus represents a case of parallel evolution from similar ancestors rather than classic convergence. A cervical-like angle of the zygapophyses has also been documented in carnivorans (Jones et al. 2020) and perissodactyls (Jones 2016). This C7 morphology is accompanied by a more vertical posture of the neck in giraffe (Danowitz and Solounias 2015) and the gerenuk (Gunji and Endo 2019), but not within the Camelidae, and seems to have evolved convergently within the long-necked lineages. However, T1 of the non-giraffid ruminants and camelids analyzed in our dataset are

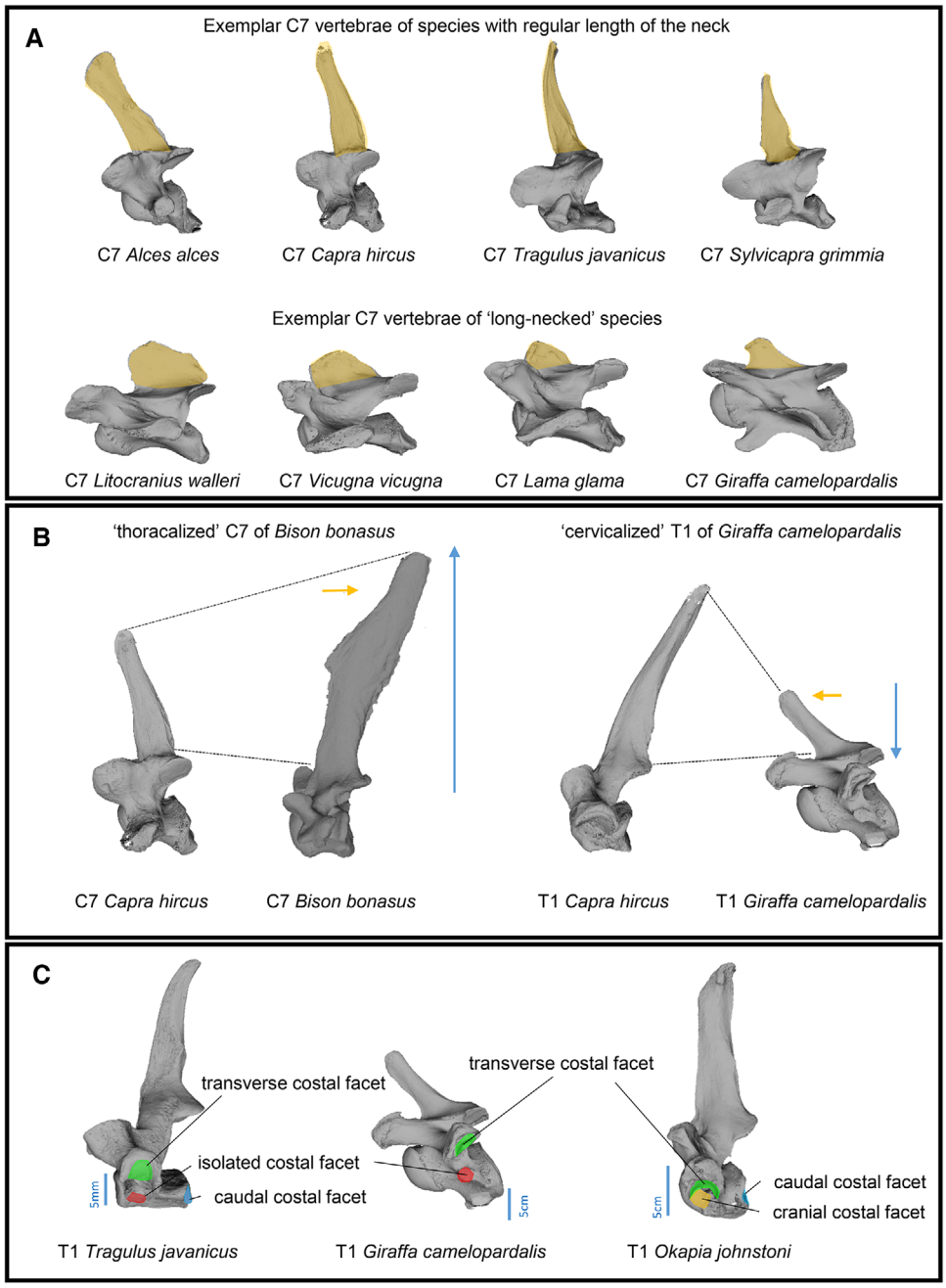

Figure 4. Morphology of the cervicothoracic vertebrae in exemplar ruminants and camelids. All specimen scaled to similar size for comparison. (A) Convergent shape evolution of C7 in "long-necked" species. (B) "Thoracalized" morphology of C7 in the European bison and "cervicalized" morphology of T1 in the giraffe in comparison to the goat (i.e., a ruminant with a "regular" neck). Yellow arrows show the inclination of the spinous process; blue arrows highlight the length of the spinous process. (C) Occurrence of isolated costal facets in the kanchil and the giraffe in comparison to the okapi (i.e., a ruminant with a "regular" neck).

inconspicuous and do not differ from species with shorter necks, whereas T1 of the giraffe clearly does.

C7 of the European bison plots outside the 95% confidence ellipse of C7 and within that of T1. The shape of C7 of the bison thus resembles the shape of a thoracic vertebra (long spinous process and short vertebral body; Fig. 4B). Shorter and wider vertebrae may help absorb high compressive forces during impacts of ramming behavior (Vander Linden and Dumont 2019). The large spinous process helps to accommodate the enormous withers in bison. Besides the "cervicalized" T1 of the giraffe, we therefore suggest a "thoracalized" C7 of the European bison. The thoracalized shape of the bison's C7 is accompanied by one of the

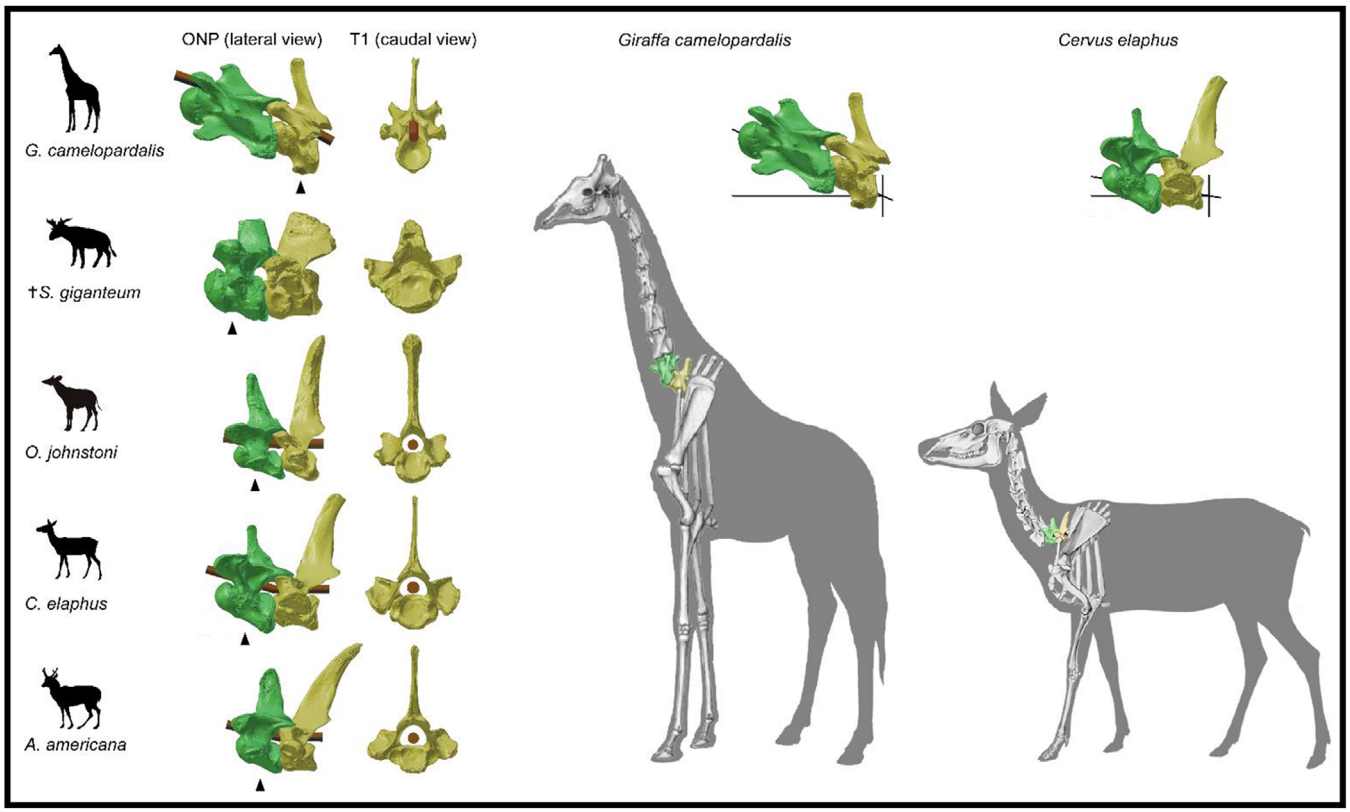

Figure 5. Dorsal inflection caused by a "keystone-shaped" vertebra at the base of the neck in exemplar species. "Keystone-shaped" vertebra appears to be T1 in the giraffe in contrast to C7 in other species and reflects the more linear posture. All vertebrae are arranged in ONP with the T1 caudal articular surface of the centrum oriented vertically.

smallest cumulative ROM between C7 and T1 of our dataset. Thus, this characteristic may be associated with an increased stabilization of the cervicothoracic transition in these short-necked and heavy-headed species displaying ramming behavior (cf. Watson et al. 2009).

We observed one species of the Tragulidae, *Tragulus javanicus* (the kanchil), showing a similar specialization in T1 with regard to the rib facets when compared with the giraffe (Fig. 4C). T1 of *T. javanicus* possesses an isolated facet beneath the transverse process and lacks the cranial costal facet. The caudal costal facet is present in the kanchil, however, which is additionally also missing in T1 of the giraffe. In the kanchil, the first rib articulates with T1 without touching the caudal part of C7, but the second rib maintains contact to the caudal part of T1. This morphological condition could, although less so than in the giraffe, again be interpreted to indicate an increased flexibility in the neck of *T. javanicus*. However, this was not supported by our ROM study, which found relatively small mobility at the cervicothoracic transition in the kanchil.

CERVICOTHORACIC TRANSITION IN *SIVATHERIUM* RESEMBLES NON-GIRAFFID SPECIES

Analysis of the cervicothoracic vertebrae of the fossil giraffid *S. giganteum* did not allow the consideration of the spinous process and other features, but nevertheless a clear separation of C7 and T1 within the morphospace was found. T1 of the giraffe clustered with the C7 of the other species in this analysis, too. The aim of this analysis was the location of the fossil giraffid *S. giganteum* in the 3D morphospace to allow a functional interpretation. C7 and T1 of the fossil plot close to other species and within the respective 95% confidence ellipses for C7 and T1. Both vertebrae plot closer to the vertebrae of the okapi than to the vertebrae of the giraffe. Danowitz and colleagues described the length-to-width ratio of C3 of *O. johnstoni*, *S. giganteum*, and other extinct giraffids as secondarily shortened compared to the primitive giraffid *Canthumeryx* sirtensis (Danowitz et al. 2015a; Danowitz et al. 2015b). Consistent with their interpretation, our findings demonstrate that 3D shapes of the vertebrae making up the cervicothoracic transition in *S. giganteum* differ from those

of the giraffe. Alternative to the interpretation of Danowitz and colleagues, the first giraffids could have been relatively short-necked and potentially acquired elongated necks independently in basal extinct giraffids such as *C. sirtensis* and extant giraffes.

IMPLICATIONS FOR NECK POSTURE

At rest, quadrupedal mammals generally hold their necks oriented more or less upright with varying degrees of curvature (Vidal et al. 1986; Fig. 5). The variation in resting neck posture appears to influence the patterns of bending moments and compressive forces in the vertebral column along the anteroposterior body axis (Christian 2002). In quadrupedal mammals with more curved necks, loads induced by the cervical vertebral column are transferred via dorsal muscles and ligaments (Slijper 1946). In bipedal mammals with less curved necks, the load almost entirely rests on the vertebral bodies. In contrast to other ruminants and camelids, the resting posture of the neck in the giraffe is relatively straight up with a forward inclination of about 30° (Christian 2002). Load induced by the head-neck system in the giraffe is transferred to a much greater degree onto the vertebral bodies than in more curved necks. Again, in addition to its functional significance in terms of mobility, the aberrant vertebral shape of the giraffe's cervicothoracic transition may thus be linked to the particular posture of the neck associated with its extreme length.

The characteristic curvature in the neck of mammals arises from the morphology of the vertebrae in undeflected state (i.e., ONP). In particular, a "keystone-shaped" vertebra at the base of the neck contributes to it (Stevens and Parrish 2005b). In mammals, this is generally C7. At ONP, the articulation between C7 and T1 creates a small inclination angle (e.g., *Cervus elaphus*) (Fig. 5). By contrast, the keystone-shaped vertebra appears to be shifted caudally from C7 to T1 in the giraffe. At ONP, the articulation between C7 and T1 forms a larger inclination angle in the giraffe. This has implications for the reconstruction of the neck posture in fossil relatives. As quantified here, the cervicothoracic transition in the fossil giraffid *S. giganteum* resembles that of the okapi more than that of the giraffe and its keystone-shaped vertebra is C7 (Fig. 5). Consequently, the neck posture of *S. giganteum* is more likely to have resembled that of the okapi and likely was not as straight as in the giraffe. Including more fossil giraffids in a future study may provide new insights into the evolution of the cervicothoracic transition in relation to total neck length. At which length and, thus, mass of the neck did the caudal shift of the keystone-shaped vertebra occur to form the relatively linear and upright neck characteristic for the modern giraffe?

Conclusion

Our quantitative analysis of 3D shape evolution of the cervicothoracic transition in cetartiodactyls demonstrates that the cervicothoracic transitions of long-necked species convergently deviate in their morphology of C7 in comparison to species with shorter necks. Their morphology is consistent with that of the giraffe's C7 (e.g., longer vertebral bodies, shorter and rather posteriorly inclined spinous processes). The exceptionally long neck of the giraffe, however, is additional supported by a unique "cervicalized" morphology of T1 characterized by a shorter, posteriorly oriented spinous process as well as a small neural arch, large cranial bulge of the articulating surface of the vertebral centrum, and a large caudal extremity (i.e., a number of homeotic changes toward a morphology that resembles that of a cervical). Indeed, these properties did result in increased quantified mobility corroborating the "functional elongation hypothesis." Moreover, T1 shape contributes to the relatively linear resting posture of the neck characteristic for giraffes. It may be interpreted as an adaptation to the particular posture of the neck associated with its exceptional length inducing large loads. We therefore suggest exploring other functional relationships than just mobility in future studies. Modeling approaches could help to better understand the aberrant vertebral morphology at the cervicothoracic transition in giraffes in terms of head-neck mass support and maintaining mobility with an elongated neck. The opposite phenomenon to the observed "cervicalization" of a thoracic vertebra also exists, as C7 of the European bison possesses a "thoracalized" morphology likely related to increased stabilization of the cervicothoracic transition. The cervicothoracic transition in the fossil giraffid *S. giganteum* is more similar to the okapi and other cetartiodactyls without a specifically long-necked morphology than to the giraffe.

AUTHOR CONTRIBUTIONS

JAN conceived of the study. MAM and CB collected 3D bone models and conducted 3D GM analysis. LM and JAN conceived and conducted ROM analysis. CB conducted statistical tests and phylogenetically informed analyses. MAM, CB, and JAN wrote the manuscript and prepared figures. All authors read and approved the final version of the manuscript.

ACKNOWLEDGMENTS

We thank K. Jones and an anonymous reviewer as well as the editors for constructive critique of earlier versions of this article. We wish to thank the following curators and collection managers for access to museum collections: C. Funk and D. Wilborn (ZMB); S. Merker (SMNS); E. Baermann (ZFMK); K. Krohmann and I. Ruf (SMF); and A. H. van Heteren and M. Hiermeier (ZSM). We thank F. Mielke and J. MacLaren (both Department of Veterinary Sciences, University of Antwerp, Belgium) for scanning the vertebral series of giraffe specimen "Dana," donated by the Koninklijke Maatschappij voor Dierkunde Centre for Research and Conservation, Antwerp, Belgium, for educational and scientific purposes. Further, we thank C. Basu and J. R. Hutchinson (The Royal Veterinary College, Structure and Motion Laboratory, Hatfield, United Kingdom) for sharing 3D surface models of Sivatherium specimens. We are indebted to K. Mahlow and M. Kirchner for their dedication and endless hours of CT scanning. We thank all

members of the "Nyakatura lab for Comparative Zoology" for inspiring and motivating discussions. This project has received funding from the European Union's Horizon 2020 research and innovation programme under grant agreement no. 8900809—EDDI (Marie-Skłodowska Curie fellowship awarded to CB). JAN acknowledges the support by the German Research Foundation (grant number EXC 2025).

DATA ARCHIVING

All 3D bone models are stored in the open access data repository MorphoMuseuM (www.morphomuseum.com). https://doi.org/10.18563/journal.m3.129 (Müller et al. 2021). All raw data and code are included as supporting information.

CONFLICT OF INTEREST

The authors declare no conflict of interest.

LITERATURE CITED

Adams, D. C. 2014. A generalized K statistic for estimating phylogenetic signal from shape and other high-dimensional multivariate data. Systematic Biology 63 : 685–697.

Adams, D. C., M. L. Collyer, A. Kaliontzopoulou, and E. Sherratt. 2017. Geomorph: Software for geometric morphometric analyses. R package version 3.0. 5.

Arnold, P. 2020. Evolution of the mammalian neck from developmental, morpho-functional, and paleontological perspectives. Journal of Mammalian Evolution. https://doi.org/10.1007/s10914-020-09506-9.

Arnold, P., M. S. Fischer, and J. A. Nyakatura. 2014. Soft tissue influence on ex vivo mobility in the hip of Iguana: comparison with in vivo movement and its bearing on joint motion of fossil sprawling tetrapods. Journal of Anatomy 225:31–41.

Arnold, P., F. Forterre, J. Lang, and M. S. Fischer. 2016. Morphological disparity, conservatism, and integration in the canine lower cervical spine: insights into mammalian neck function and regionalization. Mammalian Biology 81:153–162.

Arnold, P., E. Amson, and M. S. Fischer. 2017. Differential scaling patterns of vertebrae and the evolution of neck length in mammals. Evolution 71:1587–1599.

Badlangana, N. L., and J. W. Adams. 2009. The giraffe (Giraffa camelopardalis) cervical vertebral column: a heuristic example in understanding evolutionary processes? Zoological Journal of the Linnean Society 155:736–757.

Basu, C., P. L. Falkingham, and J. R. Hutchinson. 2016. The extinct, giant giraffid Sivatherium giganteum: skeletal reconstruction and body mass estimation. Biology Letters 12:20150940.

Basu, C., A. M. Wilson, and J. R. Hutchinson. 2019. The locomotor kinematics and ground reaction forces of walking giraffes. Journal of Experimental Biology 222:jeb159277.

Bateson, W. 1894. Materials for the study of variation. Macmillan and Co, Lond.

Belayaev, R. I., A. N. Kuznetsov, and N. E. Prilepskaya. 2020. A mechanistic approach for the calculation of intervertebral mobility in mammals based on vertebrae osteometry. J Anat 00:1–18.

Blomberg, S. P., T. Garland Jr., and A. R. Ives. 2003. Testing for phylogenetic signal in comparative data: behavioral traits are more labile. Evolution 57:717–745.

Böhmer, C. 2017. Correlation between Hox code and vertebral morphology in the mouse: towards a universal model for Synapsida. Zoological Letters 3:, 1–11.

Böhmer, C., E. Amson, P. Arnold, A. H. Van Heteren, and J. A. Nyakatura. 2018. Homeotic transformations reflect departure from the mammalian 'rule of seven' cervical vertebrae in sloths: inferences on the Hox code and morphological modularity of the mammalian neck. BMC Evolutionary Biology 18:84.

Bookstein, F. L., 1997. Morphometric tools for landmark data: geometry and biology, Cambridge University Press, Cambridge, MA.

Chen, F., J. Greer, and M. R. Capecchi. 1998. Analysis of Hoxa7/Hoxb7 mutants suggests periodicity in the generation of the different sets of vertebrae. Mech. Dev 77:49–57.

Christian, A. 2002. Neck posture and overall body design in sauropods. Mitteilungen des Museums für Naturkunde Berlin Geowissenschaftliche Reihe 5:271–281.

Cignioni, M. J., M. Callieri, M. Corsini, M. Dellepiane, F. Ganovelli, and G. Ranzuglia. 2008. Meshlab: an open-source mesh processing tool. https://doi.org/10.2312/LocalChapterEvents/ItalChap/ItalianChapConf2008/129-136.

Cobley, M. J., E. J. Rayfield, and P. M. Barrett. 2013. Inter-vertebral flexibility of the ostrich neck: implications for estimating sauropod neck flexibility. PLoS One 8:e72187.

Cramer, G. D., and S. A. Darby. 2014. Clinical anatomy of the spine, Spinal Cord and ANS, Mosby, St. Louis, MO.

Damian, A., A. Gudea, A. Blendea, I. Ciama, F. Tuns, and I. Irimescu. 2013. Study of the axial skeleton in the giraffe (Giraffa camelopardalis) compared to its bovine counterpart. Sci Works, C Ser, Vet Med 58:90–99.

Danowitz, M., and N. Solounias. 2015. The cervical osteology of Okapia johnstoni and Giraffa camelopardalis. PLoS ONE 10:e0136552.

Danowitz, M., R. Domalski, and N. Solounias. 2015a. The cervical anatomy of Samotherium, an intermediate-necked giraffid. Royal Society Open Science 2:150521.

Danowitz, M., A. Vasilyev, V. Kortlandt, and N. Solounias. 2015b. Fossil evidence and stages of elongation of the Giraffa camelopardalis neck. Royal Society Open Science 2:150393.

Flower, W. H., and H. Gadow. 1885. An introduction to the osteology of the Mammalia, Macmillan, New York.

Goethe, J. W. 2012. Naturwissenschaftliche Schriften I – Morphologie. 14th ed. In E. Trunz, CH Beck (eds.), Werke. Hamburger Ausgabe, Munich.

Gower, J. C. 1975. Generalized procrustes analysis. Psychometrika 40:33–51.

Gunji, M., and H. Endo. 2016. Functional cervicothoracic boundary modified by anatomical shifts in the neck of giraffes. Royal Society Open Science 3:150604.

———. 2019. Growth pattern and functional morphology of the cervical vertebrae in the Gerenuk (*Litocranius walleri*): the evolution of neck elongation in Antilopini (Bovidae, Artiodactyla). Journal of Mammal Evolution 26:225–235.

Harvey, P. H., and M. D. Pagel. 1991. The comparative method in evolutionary biology. Oxford University Press, Oxford, U.K.

Jolliffe, I. 2011. Principal component analysis. Springer, Berlin.

Jones, K. E. 2016. Preliminary data on the effect of osseous anatomy on ex vivo joint mobility in the equine thoracolumbar region. Equine Veterinary Journal 48:502–508.

Jones, K. E., K. D. Angielczyk, P. D. Polly, J. J. Head, V. Fernandez, J. K. Lungmus, S. Tulga, and S. E. Pierce. 2018. Science 361:1249–1252.

Jones, K. E., S. Gonzales, K. D. Angielczyk, and S. E. Pierce. 2020. Regionalization of the axial skeleton predates functional adaptation in the forerunners of mammals. Nature Ecology & Evolution 4.3:470–478.

Krings, M., J. A. Nyakatura, M. S. Fischer, and H. Wagner. 2014. The cervical spine of the American barn owl (*Tyto furcata pratincola*): I. Anatomy of the vertebrae and regionalization in their S-shaped arrangement. PLoS ONE 9:e91653.

Krings, M., J. A. Nyakatura, M. L. Boumans, M. S. Fischer, and H. Wagner. 2017. Barn owls maximize head rotations by a combination of yawing and rolling in functionally diverse regions of the neck. Journal of Anatomy 231:12–22.

Kuznetsov, A. N., and V. S. Tereschenko. 2010. A method for estimation of lateral and vertical mobility of platycoelous vertebrae of tetrapods. Paleontology Journal 44:209–225.

Lankester, R. 1908. On certain points in the structure of the cervical vertebrae of the okapi and the giraffe. Proceedings of the Zoological Society of London 78:320–334.

Loscher, D. M., F. Meyer, K. Kracht, and J. A. Nyakatura. 2016. Timing of head movements is consistent with energy minimization in walking ungulates. Proceedings of the Royal Society B: Biological Sciences 283:20161908.

Manafzadeh, A. R., and K. Padian. 2018. ROM mapping of ligamentous constraints on avian hip mobility: implications for extinct ornithodirans. Proceedings of the Royal Society B: Biological Sciences 285:20180727.

Manafzadeh, A. R., and S. M. Gatesy. 2020. A coordinate-system-independent method for comparing joint rotational mobilities. Journal of Experimental Biology. https://doi.org/10.1242/jeb.227108.

Mitchell, G., and J. D. Skinner. 2003. On the origin, evolution and phylogeny of giraffes Giraffa camelopardalis. Transactions of the Royal Society of Africa 58:51–73.

Müller, M. A., L. Merten, C. Böhmer, and J. A. Nyakatura, 2021. 3D models related to the publication: Pushing the boundary? Testing the 'functional elongation hypothesis' of the giraffe's neck. MorphoMuseuM 6:e129. https://doi.org/10.18563/journal.m3.129.

Nyakatura, J. A., V. R. Allen, J. Lauströer, A. Andikfar, M. Danczak, H. J. Ullrich, W. Hufenbach, T. Martens, and M. S. Fischer. 2015. A three-dimensional skeletal reconstruction of the stem amniote Orobates pabsti (Diadectidae): analyses of body mass, centre of mass position, and joint mobility. PLoS ONE 10:e0137284.

Nyakatura, J. A., K. Melo, T. Horvat, K. Karakasiliotis, V. R. Allen, A. Andikfar, E. Andrada, P. Arnold, J. Lauströer, J. R. Hutchinson, et al. 2019. Reverse-engineering the locomotion of a stem amniote. Nature 565:351–356.

Owen, R. 1866. On the anatomy of vertebrates: volume 2, birds and mammals. Longmans, Green and Company, Harlow, U.K.

O'higgins, P. 2000. The study of morphological variation in the hominid fossil record: biology, landmarks and geometry. The Journal of Anatomy 197:103–120.

Pierce, S. E., J. A. Clack, and J. R. Hutchinson. 2012. Three-dimensional limb joint mobility in the early tetrapod Ichthyostega. Nature 486:523–526.

R Development Core Team. 2019. R: A language and environment for statistical computing. R Foundation for Statistical Computing, Vienna.

Randau, M., A. R. Cuff, J. R. Hutchinson, S. E. Pierce, and A. Goswami. 2017. Regional differentiation of felid vertebral column evolution: a study of 3D shape trajectories. Organisms Diversity & Evolution 17:305–319.

Regnault, S., and S. E. Pierce. 2018. Pectoral girdle and forelimb musculoskeletal function in the echidna (*Tachyglossus aculeatus*): insights into mammalian locomotor evolution. Royal Society Open Science 5:181400.

Reljić, I., I. Dunder, and S. Seljan. 2019. Photogrammetric 3D scanning of physical objects: tools and workflow. TEM Journal 8:383–388.

Revell, L. J. 2012. phytools: an R package for phylogenetic comparative biology (and other things). Methods in Ecology and Evolution 3:217–223.

Rohlf, F. J. & Corti, M. 2000. Use of two-block partial least-squares to study covariation in shape. Systematic Biology 49:740–753.

Rohlf, F. J., and D. Slice. 1990. Extensions of the Procrustes method for the optimal superimposition of landmarks. Systematic Biology 39:40–59.

Schindelin, J., I. Arganda-Carreras, E. Frise, V. Kaynig, M. Longair, T. Pietzsch, S. Preibisch, C. Rueden, S. Saalfeld, B. Schmid, et al. 2012. Fiji: an open source platform for biological-image analysis. Nature Methods 9:676–682.

Schneider, C., W. Rasband, and K. Eliceiri. 2012. NIH image to ImageJ: 25 years of image analysis. Nature Methods 9:671–675.

Sidlauskas, B. 2008. Continuous and arrested morphological diversification in sister clades of characiform fishes: a phylomorphospace approach. Evolution: International Journal of Organic Evolution 62:3135–3156.

Simmons, R. E., and L. Scheepers. 1996. Winning by a neck: sexual selection in the evolution of the giraffe. The American Naturalist 148:771–786.

Slijper, E. J. 1946. Comparative biologic-anatomical investigation on the vertebral column and spinal musculature of mammals. North-Holland Publishing Company, Amsterdam, Netherlands.

Solounias, N. 1999. The remarkable anatomy of the giraffe's neck. Journal of Zoology 247:257–268.

Stalling, D., M. Westerhoff, and H.-C. Hege. 2005. Amira: a highly interactive system for visual data analysis. The Visualization Handbook 38:749-767.

Stayton, C. T. 2006. Testing hypotheses of convergence with multivariate data: morphological and functional convergence among herbivorous lizards. Evolution 60:824–841.

———. 2015. The definition, recognition, and interpretation of convergent evolution, and two new measures for quantifying and assessing the significance of convergence. Evolution 69:2140–2153. https://doi.org/10.1111/evo.12729.

———. 2017. Convevol: analysis of convergent evolution. R package. Available via https://cran.r-project.org/package=convevol.

Stevens, K. A., and J. M. Parrish. 2005a. Digital reconstructions of sauropod dinosaurs and implications for feeding. Pp. 178–200 *in* K. A. Curry Rogers and J. A. Wilson, eds. The sauropods: evolution and paleobiology. University of California Press, Berkeley, CA.

Stevens, K. A., and J. M. Parrish. 2005b. Neck posture, dentition, and feeding strategies in Jurassic sauropod dinosaurs. Pp. 212–232 *in* V. Tidwell and K. Carpenter, eds. Thunder-lizards: the sauropodomorph dinosaurs. Indiana Univ. Press, Bloomington, IN.

Taylor, M. P., and M. J. Wedel. 2013. The effect of intervertebral cartilage on neutral posture and range of motion in the necks of sauropod dinosaurs. PLoS One 8:e78214.

Toljagic, O., K. L. Voje, M. Matschiner, L. H. Liow, and T. F. Hansen. 2018. Millions of years behind: slow adaptation of ruminants to grasslands. Systematic Biology 67:145–157.

Van Sittert, S. J., J. D. Skinner, and G. Mitchell. 2010. From fetus to adults – an allometric analysis of the giraffe vertebral column. Journal of Experimental Zoology Part B: Molecular and Developmental Evolution 314:469–479.

Vander Linden, A., and E. R. Dumont. 2019. Intraspecific male combat behavior predicts morphology of cervical vertebrae in ruminant mammals. Proceedings of the Royal Society London B 286:20192199.

Vidal, P. P., W. Graf, and A. Berthoz. 1986. The orientation of the cervical vertebral column in unrestrained awake animals. Experimental Brain Research 61:549–559.

Vidal, D., P. Mocho, A. Páramo, J. L. Sanz, and F. Ortega. 2020. Ontogenetic similarities between giraffe and sauropod neck osteological mobility. PLoS One 15:e0227537.

Watson, C., G. Paxinos, and G. Kayalioglu. 2009. The spinal cord: a Christopher and Dana Reeve Foundation text and atlas. Academic Press, Cambridge, MA.

Wellik, D. M. 2009. Hox genes and vertebrate axial pattern. Current Topics in Developmental Biology 88:257–278.

Wiley, D. F., N. Amenta, D. A. Alcantara, D. Ghosh, Y. J. Kil, E. Delson, W. Harcourtsmith, R. J. Rohlf, K. St John, and B. Hamann. 2005. Evolutionary morphing. Proceedings of the IEEE Visualization 2005:431–438.

Zelditch, M. L., D. L. Swiderski, H. D. Sheets, and W. L. Fink. 2004. Geometric morphometrics for biologists: a primer. Elsevier Academic Press, New York.

Associate Editor: A. Kaliontzopoulou
Handling Editor: A.G. McAdam

Supporting Information

Additional supporting information may be found online in the Supporting Information section at the end of the article.

Supplementary Material

SI 1: Complete specimen list.

SI 2: Overview of C7/T1 pairs for all 38 species analyzed.

SI 3: 3D surface models of fossil giraffid *Sivatherium giganteum*.

SI 4: Comparison of digitization method (μCT vs. photogrammetry).

SI 5: Range of motion and relative neck length (largest values in bold print).

SI 6: Morphology of vertebra and definition of landmarks (landmark set used in this study shown on C7 of *Giraffa camelopardalis* ZMB 66393).

SI 7: Landmark definitions. Definitions follow Arnold et al. (2016).

SI 8: Assessment of range of motion (ROM) using 3D bone models.

SI 9: PC plots (PC3 vs. PC4) for the full landmark set (A) and the adjusted landmark set (SI 6) using only those landmarks that were identifiable also on the fossil specimens (B).

SI 10: Principal components of analyses that explain a cumulative variance of 95%. A: Analysis of cervicothoracic transition (C7. T1).

SI 11: Renderings of C7 (green) and T1 (yellow) pairs to illustrate cumulative range of motion in exemplar species.

SI 12: Morphological traits at the cervicothoracic transition in giraffe and okapi demonstrates homeotic shifts (number of apparent cranial steps in cervical count) in the giraffe neck.